Bioactive Materials 47 (2025) 448–459

Contents lists available at ScienceDirect

Bioactive Materials

journal homepage: www.keaipublishing.com/en/journals/bioactive-materials

Polymer-modified DNA hydrogels for living mitochondria and nanozyme delivery in the treatment of rheumatoid arthritis

Fuxiao Wang [a,c,e,f,1], Yafei Han [a,c,1], Qirong Zhou [b,1], Shihao Sheng [b,1], Yan Hu [b], Hao Zhang [b], Xiao Chen [b], Chongru He [b,**], Hongbo Tan [g,***], Long Bai [a,c,d,****], Jiacan Su [a,b,c,*]

[a] Organoid Research Center, Institute of Translational Medicine, Shanghai University, Shanghai 200444, China
[b] Department of Orthopedics, Xinhua Hospital Affiliated to Shanghai Jiao Tong University School of Medicine, Shanghai, 200092, China
[c] National Center for Translational Medicine (Shanghai) SHU Branch, Shanghai University, Shanghai 200444, China
[d] Wenzhou Institute of Shanghai University, Wenzhou, Zhejiang, China
[e] School of Medicine, Shanghai University, Shanghai, 200444, China
[f] School of Environmental and Chemical Engineering, Shanghai University, Shanghai, 200444, China
[g] Department of Orthopaedics, People's Liberation Army Joint Logistic Support Force 920th Hospital, Kunming City, Yunnan Province, China

ARTICLE INFO

Keywords:
DNA hydrogel
Mitochondrial delivery
Nanozyme
Mitochondrial renewal
Rheumatoid arthritis

ABSTRACT

Rheumatoid arthritis (RA) is a chronic autoimmune disease that leads to joint deformities and functional impairments. Traditional treatment approaches, such as nonsteroidal anti-inflammatory drugs, disease-modifying antirheumatic drugs, and molecular targeted therapies, often fail to simultaneously achieve efficient inflammation relief and cartilage tissue repair. DNA hydrogels, derived from nucleic acid nanotechnology, have demonstrated potential in RA therapy due to their programmability, high biocompatibility, and tunable degradation properties. However, their application is still hindered by challenges including high synthesis costs, immunogenicity risks, and uncontrolled degradation rates. To address these limitations, this study proposes a dual-action strategy involving a polymer-modified DNA hydrogel co-delivering nanozymes and living mitochondria to overcome the constraints of traditional therapies and comprehensively optimize RA treatment outcomes. The incorporation of functionalized polymers significantly reduces synthesis costs and immunogenicity while fine-tuning the degradation rate of the hydrogel, enabling sustained support during bone and cartilage repair. The hydrogel is loaded with Prussian blue nanozymes to scavenge excessive reactive oxygen species (ROS) within the RA microenvironment, alleviating inflammation, and facilitates intracellular delivery of living mitochondria to inhibit ROS production at its source, promoting tissue repair. By integrating endogenous ROS reduction with exogenous ROS clearance, this strategy markedly enhances therapeutic efficacy, offering a novel approach for precise RA treatment and advancing the clinical translation of biomaterials.

1. Introduction

Rheumatoid arthritis (RA) is a chronic autoimmune disease marked by persistent inflammation of the synovial membrane, joint damage [1], and eventual loss of joint function, severely diminishing patients' quality of life [2]. Conventional therapies, such as nonsteroidal anti-inflammatory drugs, glucocorticoids, and disease-modifying antirheumatic drugs, provide symptomatic relief but are often associated with adverse effects and fail to address the underlying disease progression [3].

Hydrogels, with their high water content, superior biocompatibility, and adjustable mechanical properties, have demonstrated substantial potential in the fields of tissue engineering and regenerative medicine [4]. They enable localized and sustained drug delivery while providing a

* Corresponding authors. Organoid Research Center, Institute of Translational Medicine, Shanghai University, Shanghai 200444, China.
** Corresponding author.
*** Corresponding authors.
**** Corresponding author. Organoid Research Center, Institute of Translational Medicine, Shanghai University, Shanghai 200444, China.
E-mail addresses: hechongru@163.com (C. He), tantoo@163.com (H. Tan), bailong@shu.edu.cn (L. Bai), drsujiacan@163.com (J. Su).
[1] The four authors contributed equally to this work.

https://doi.org/10.1016/j.bioactmat.2024.12.027
Received 3 December 2024; Received in revised form 25 December 2024; Accepted 26 December 2024

microenvironment conducive to cell proliferation and tissue repair [5]. DNA hydrogels, which are engineered using nucleic acid nanotechnology, exhibit unique advantages such as programmability and tunable degradation profiles, making them promising candidates for RA therapy [6]. Nevertheless, their application is constrained by challenges including high production costs, potential immunogenic responses, and limited control over degradation kinetics.

To overcome these challenges, we introduce a polymer-modified DNA hydrogel. The incorporation of a functionalized polymer network substantially reduces the requirement for high concentrations of oligonucleotides, thereby significantly decreasing the associated synthesis costs. Moreover, the polymer modification effectively masks the immunologically active sites of DNA, thereby minimizing the risk of immunogenicity. Additionally, the degradation rate of the hydrogel is precisely modulated by adjusting the crosslinking density of the polymer and the degradable chemical bonds, ensuring temporal compatibility with the structural support demands during bone and cartilage repair processes.

However, relying solely on polymer-modified DNA hydrogels may be insufficient to fully address the complex pathological features of RA.

In the pathological environment of RA, ROS levels are significantly elevated, driving oxidative stress that amplifies inflammation and tissue damage. Pro-inflammatory cytokines such as TNF-α and IL-1β activate M1 macrophages, which produce excessive ROS, further promoting cartilage degradation and bone resorption through the activation of MMPs and osteoclasts. Nanozymes [7], as a class of nanomaterials with enzyme-like catalytic activities, have gained attention due to their high stability, cost-effectiveness, and scalability. Among them, Prussian blue nanozymes have been particularly recognized for their exceptional ROS-scavenging capabilities [8,9]. Studies have demonstrated that Prussian blue nanozymes can effectively eliminate excessive ROS in the RA microenvironment, thereby mitigating inflammatory responses [10].

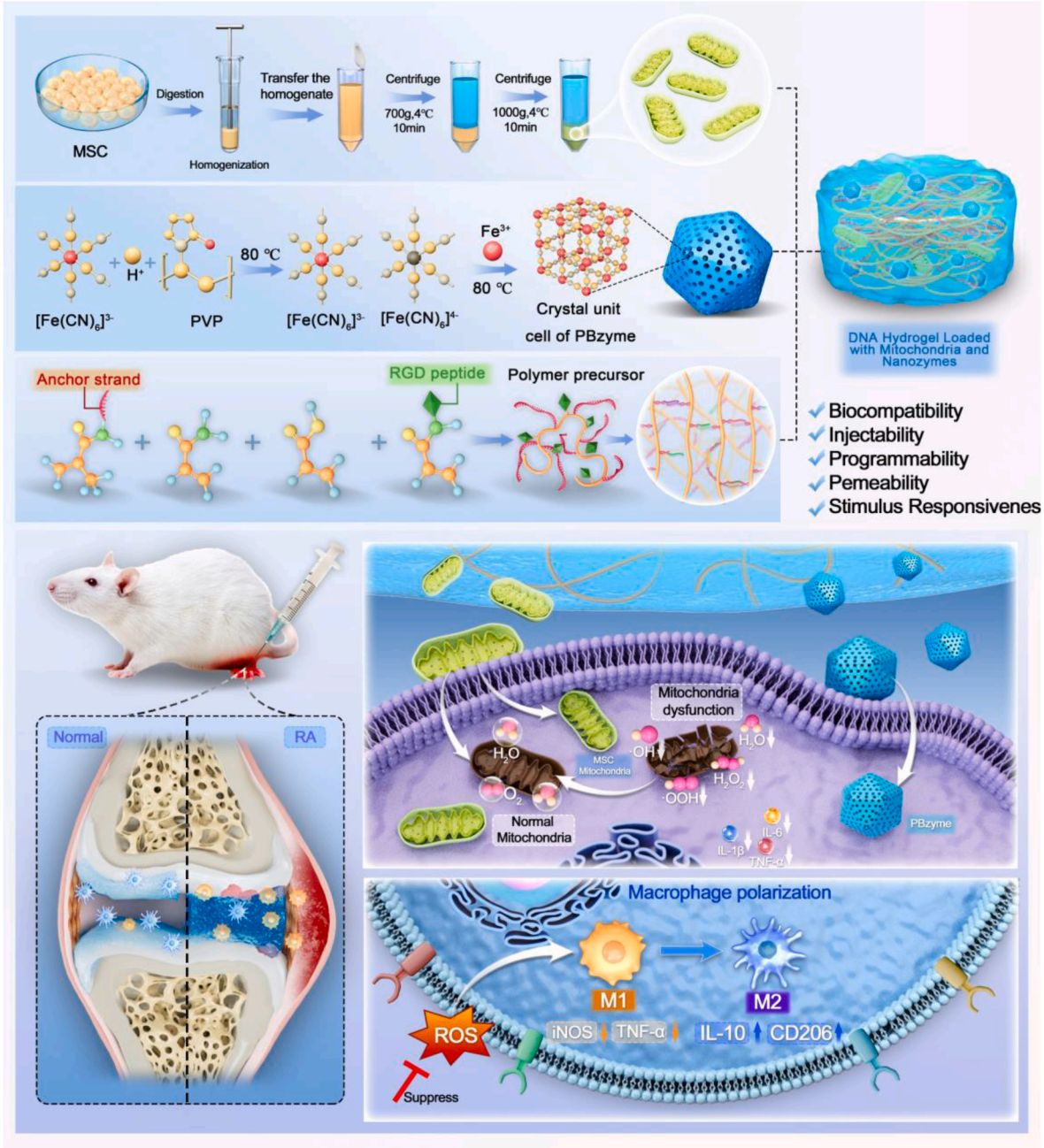

Fig. 1. Schematic of the preparation process of DNA hydrogel loaded with MSC-Mitochondria and nanozymes and its application in RA treatment.

However, given the persistent production of ROS caused by mitochondrial dysfunction in RA, merely clearing extracellular ROS may be insufficient to achieve a comprehensive therapeutic outcome [11,12].

Mitochondrial transfer, as an emerging therapeutic strategy, offers a novel approach to addressing metabolic dysregulation in RA [13]. By transferring living mitochondria, defined as functionally active and biologically viable mitochondria capable of restoring cellular energy metabolism and supporting cellular function in recipient cells, this strategy helps reduce the production of pro-inflammatory cytokines [14]. For instance, studies have demonstrated that mitochondrial

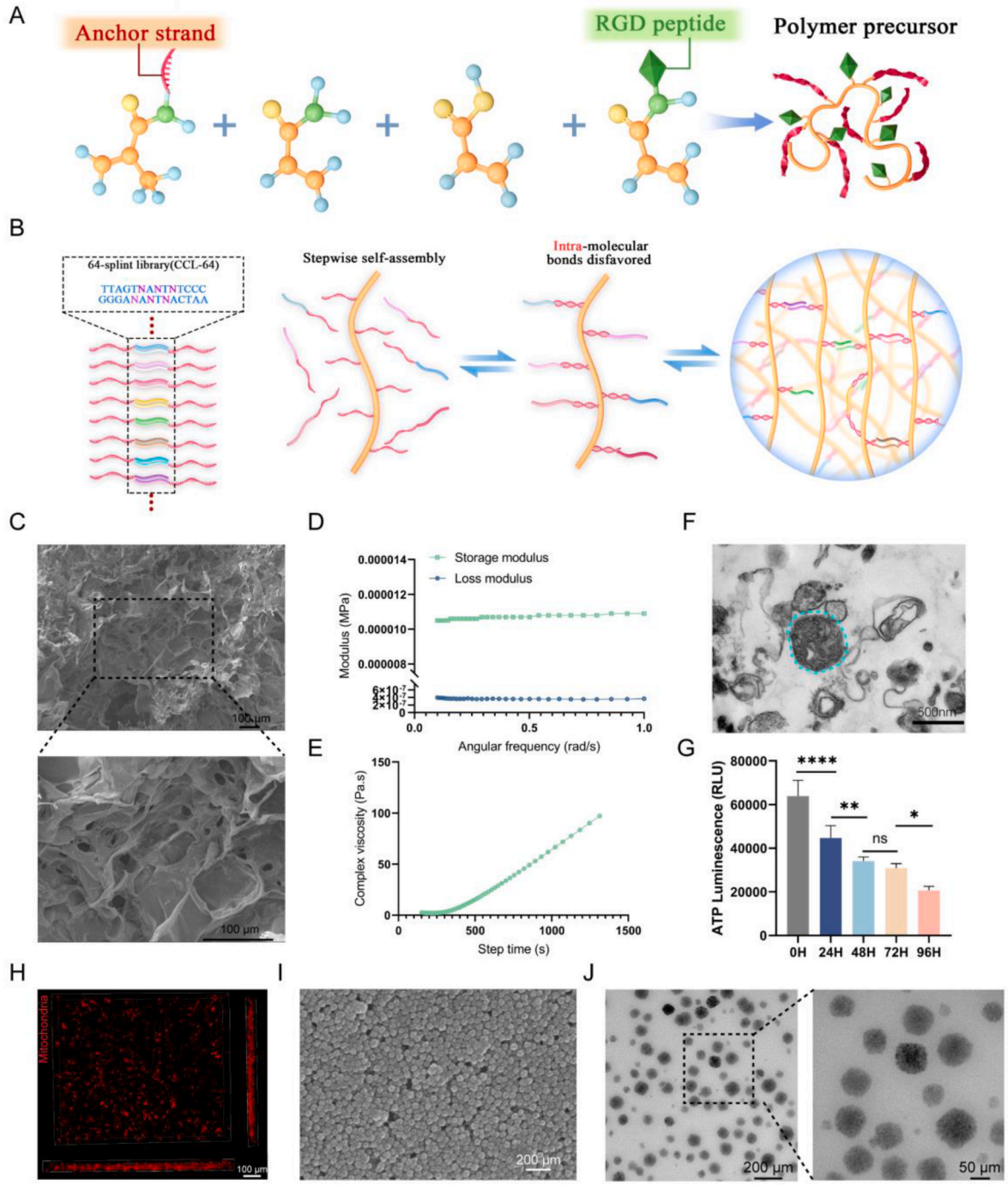

Fig. 2. Preparation and Characterization of DNA Hydrogel Loaded with MSC-Mitochondria and Nanozymes. (A–B) Schematic representation of the DNA hydrogel polymer precursor and its crosslinking process. Panel A illustrates the design of the DNA hydrogel precursor, including the assembly of DNA strands and the introduction of crosslinking agents. Panel B depicts the crosslinking process that occurs when the DNA strands are linked together under specific conditions, forming a stable hydrogel network. (C) SEM image of the porous DNA hydrogel (Scale bar: 100 μm). (D) Rheological properties of the DNA hydrogel showing storage modulus (G') and loss modulus (G''). (E) Complex viscosity curve of the DNA hydrogel, illustrating the flow behavior of the hydrogel under varying shear rates. This plot provides insights into the viscoelastic properties of the material, indicating its suitability for injectable applications and its ability to maintain consistency upon administration. (F) TEM image of extracted mitochondria (Scale bar: 500 nm). (G) ATP assay of extracted mitochondria showing high activity immediately after extraction, with significant decline after prolonged storage at −80 °C, confirming the use of fresh mitochondria in our experiments. (H) Fluorescence imaging showing uniform distribution of mitochondria within the DNA hydrogel, ensuring efficient release for therapeutic delivery. (I) SEM image of the synthesized nanozyme (Scale bar: 200 μm). (J) TEM image of the synthesized nanozyme (Scale bar: 200 μm (left) and 50 μm (right)).

transfer can enhance functional angiogenesis in ischemic tissues, providing a promising therapeutic option for ischemic diseases [15]. In this study, we innovatively combined mitochondrial transfer with nanozyme therapy to establish a dual mechanism: efficient extracellular ROS scavenging by nanozymes and intracellular ROS suppression through mitochondrial transfer. This dual-action strategy aims to restore energy homeostasis in the joint microenvironment, ultimately achieving effective inflammation resolution.

Building on these, we designed and synthesized a polymer-modified DNA hydrogel co-loaded with prussian blue nanozymes and functional, healthy mitochondria. This composite hydrogel not only efficiently scavenges ROS in the RA microenvironment to alleviate inflammation but also leverages mitochondrial transfer to restore cellular energy metabolism and reduce endogenous ROS production. Both *in vitro* experiments and animal studies demonstrated its significant efficacy in promoting chondrocyte proliferation and differentiation, alleviating RA symptoms, and repairing joint tissue (Fig. 1).

In summary, this study introduces an innovative strategy that integrates nanozyme therapy with mitochondrial transfer for comprehensive RA treatment. This approach highlights the potential and prospects of biomaterials in precision medicine. The combination not only enhances therapeutic outcomes but also offers a novel method for clinical RA management, holding promise to provide more effective treatment options for RA patients. In addition, this technology holds significant potential for application in other related diseases. For example, in conditions characterized by excessive ROS production and mitochondrial dysfunction, such as neurodegenerative and cardiovascular diseases, this strategy could prove similarly effective. By eliminating excess ROS and restoring mitochondrial function, it may alleviate disease symptoms and improve patient outcomes. Therefore, this study not only provides a novel therapeutic approach for RA but also explores new possibilities for the treatment of other related diseases.

2. Results

2.1. Preparation and characterization of DNA hydrogel loaded with mitochondria and nanozyme

The DNA hydrogel was synthesized by integrating anchor DNA strands within an acrylamide matrix, followed by polymerization to form a three-dimensional polymeric network. Crosslinking was achieved using complementary DNA strands through Watson-Crick base pairing, yielding a hydrogel with robust structural integrity and tunable mechanical properties. RGD peptides promote cell adhesion to the DNA hydrogel, making it easier for cells to internalize mitochondria and nanozymes (Fig. 2A and B). The synthesized hydrogel was subsequently characterized to confirm its suitability for encapsulating mitochondria and nanozymes.

The scanning electron microscopy (SEM) image of the DNA hydrogel revealed a porous microarchitecture (Fig. 2C), which is critical for ensuring high encapsulation capacity and facilitating the controlled release of therapeutic agents. Rheological analysis demonstrated that the hydrogel maintained a solid-like behavior, as evidenced by the storage modulus (G') exceeding the loss modulus (G'') over a wide frequency range (Fig. 2D). During the gelation process, the gradual increase in the complex viscosity of DNA hydrogel provides a dynamic, stable, and tunable culture environment for cells (Fig. 2E). This property facilitates uniform cell encapsulation and distribution while allowing the mechanical properties of the hydrogel to adapt, effectively mimicking the in vivo microenvironment. Such characteristics support cell adhesion, proliferation, and differentiation, making DNA hydrogel an ideal biomaterial for tissue engineering applications. The porous structure of the DNA hydrogel facilitated the successful encapsulation of mitochondria and nanozymes. The TEM image of the extracted mitochondria confirmed their intact morphology (Fig. 2F). Additionally, we validated the activity of the extracted mitochondria *in vitro*. ATP assay results demonstrated that mitochondria retained high activity immediately after extraction (Fig. 2G). However, prolonged storage at −80 °C led to a significant decrease in mitochondrial activity. Therefore, in our experiments, we adhered to the principle of utilizing mitochondria in their fresh state. Furthermore, we observed the distribution of mitochondria within the DNA hydrogel, and fluorescence imaging revealed a homogeneous distribution of mitochondria in the hydrogel, which is conducive to their efficient release (Fig. 2H). And the TEM and SEM image of the synthesized nanozyme illustrated its uniform particle size and surface morphology (Fig. 2I and J), supporting its functional stability.

These results validate the successful synthesis and characterization of a DNA hydrogel with favorable properties for biomedical applications. Its structural and rheological characteristics make it an ideal carrier for therapeutic agents, paving the way for innovative approaches in targeted drug delivery and tissue regeneration.

2.2. Functional validation of composites in vitro

After successfully constructing the composite material system, we initially evaluated its biocompatibility. The experiment was divided into five groups: control, DNA hydrogel, nanozyme, mitochondria, and composite material which named DN-Mito (DNA hydrogel + nanozyme + mitochondria). Live/dead cell staining results (Fig. 3A) indicated that Raw264.7 cells exhibited good viability across all groups, demonstrating the excellent biocompatibility of the materials. Similarly, cytoskeletal staining results (Fig. 3B) revealed normal cell morphology in all groups, suggesting that the components did not adversely affect cell viability. Additionally, cell proliferation activity was assessed using the CCK-8 assay. The results (Fig. S1 A) showed that both the mitochondria-only group and the composite material group containing mitochondria significantly enhanced the proliferation of Raw264.7 macrophages compared to the control group. Collectively, these findings confirm that the individual components of the composite material exhibit good biocompatibility with macrophages and promote cell proliferation.

To investigate the role of mitochondria in immune regulation, particularly their anti-inflammatory potential in macrophages, we first fluorescently labeled the isolated mitochondria using mitochondrial staining kit. The labeled mitochondria were then co-cultured with 1 million macrophages for 24 h. Confocal fluorescence microscopy revealed the presence of red fluorescently labeled mitochondria surrounding the macrophage nuclei, clearly indicating the successful uptake of exogenous mitochondria by the macrophages (Fig. 4A). Furthermore, when mitochondria were transferred to cells without prior labeling, the mitochondrial transfer group exhibited a significantly higher mitochondrial count compared to other groups (Fig. 4B and Fig. S2A). We next assessed the mitochondrial membrane potential. Mitochondrial damage was induced by LPS treatment, and the control group showed a significant reduction in mitochondrial membrane potential. The DNA hydrogel alone did not improve membrane potential. However, the addition of nanozymes and mitochondria resulted in a significant restoration of mitochondrial membrane potential, with the combined use of both showing the most effective improvement (Fig. 4C and D).

Mitochondrial homeostasis is closely intertwined with cellular energy metabolism and plays a pivotal role in various cellular processes, including macrophage polarization and the expression of inflammatory cytokines. Modulating mitochondrial metabolism can influence macrophage polarization, thereby affecting immune responses and the expression of inflammatory cytokines. In our study, M1 macrophages were identified by red fluorescent labeling of iNOS, characterized by a "round, spiky" morphology, while M2 macrophages were identified by green fluorescent labeling of CD206, exhibiting a "spindle-shaped" morphology. The experimental results (Fig. 4E) demonstrated that in the control and DNA hydrogel groups, macrophages predominantly exhibited an M1 phenotype. In contrast, an increase in M2 macrophages

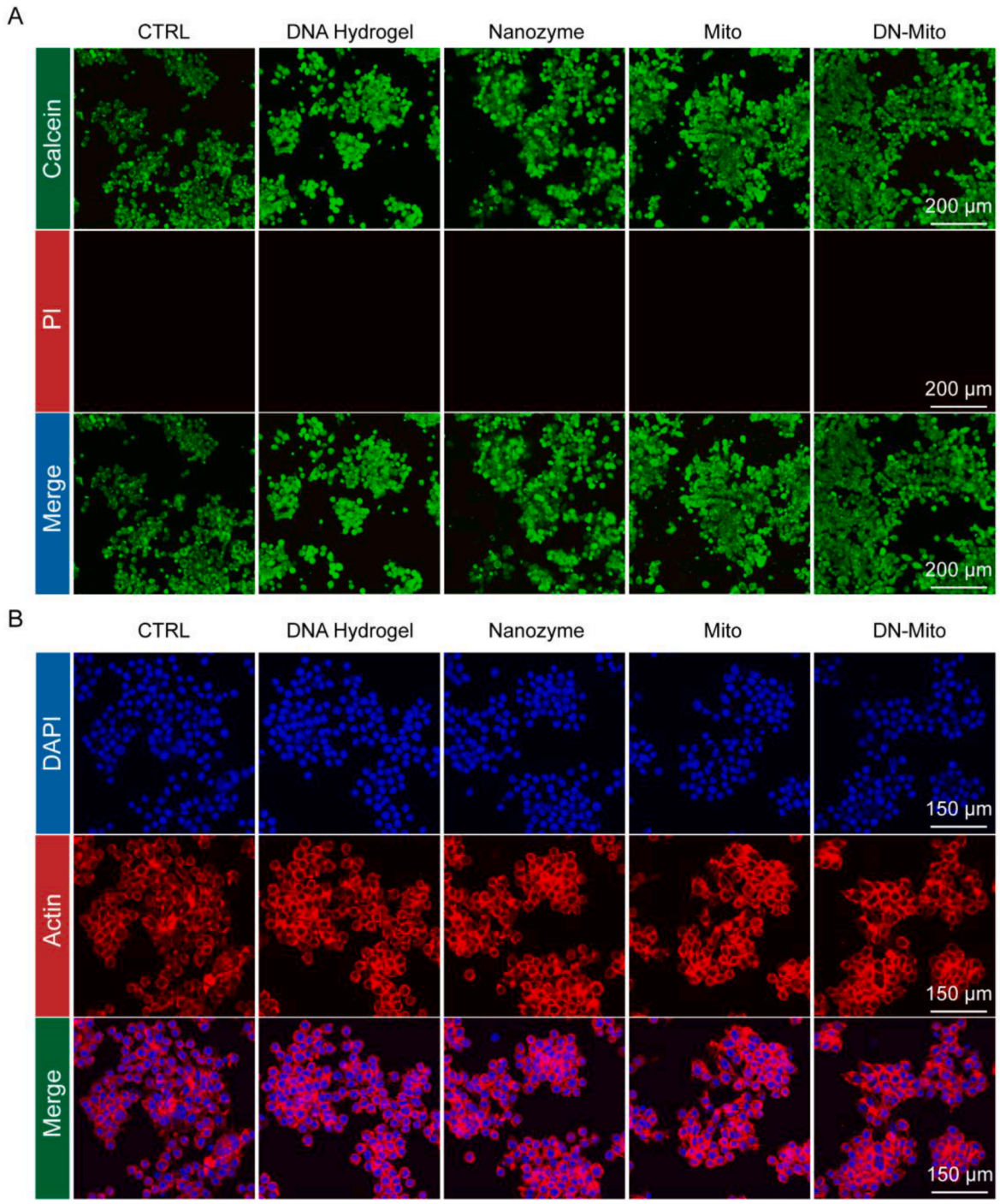

Fig. 3. Biocompatibility and Proliferation Assessment of the Composite Material System on Raw264.7 Macrophages. (A) Cell viability following various treatments was assessed using propidium iodide (PI) and Calcein AM staining. Calcein AM stains live cells with intact cell membranes, emitting green fluorescence, while PI stains dead or permeabilized cells with red fluorescence. (Scale bar: 200 μm). (B) Cytoskeleton staining of macrophages in different treatment groups, highlighting the morphological changes of the cells. Actin filaments were stained with Phalloidin, and the nuclei were counterstained with DAPI to show the overall cell structure. (Scale bar: 150 μm).

was observed in the nanozyme-treated group. The group treated with exogenous mitochondria showed an even higher number of M2 macrophages. Most notably, the composite material group containing both exogenous mitochondria and nanozymes exhibited the highest number of M2 macrophages. Subsequently, we explored the anti-inflammatory effects of different experimental materials by inducing an inflammatory response in Raw264.7 macrophages using LPS and measuring the expression of inflammatory cytokines IL-1β, IL-6, and TNF-α via PCR. The results (Fig. 4F) revealed that compared to the control group, the nanozyme-treated group displayed reduced levels of inflammatory cytokines. The reduction was more pronounced in the group treated with exogenous mitochondria. However, the composite material group combining nanozymes and exogenous mitochondria exhibited the strongest inhibition of inflammatory cytokine expression.

These findings underscore the potential role of exogenous mitochondria in modulating immune responses and suppressing inflammation, while also confirming the anti-inflammatory properties of nanozymes. More importantly, the combination of nanozymes and

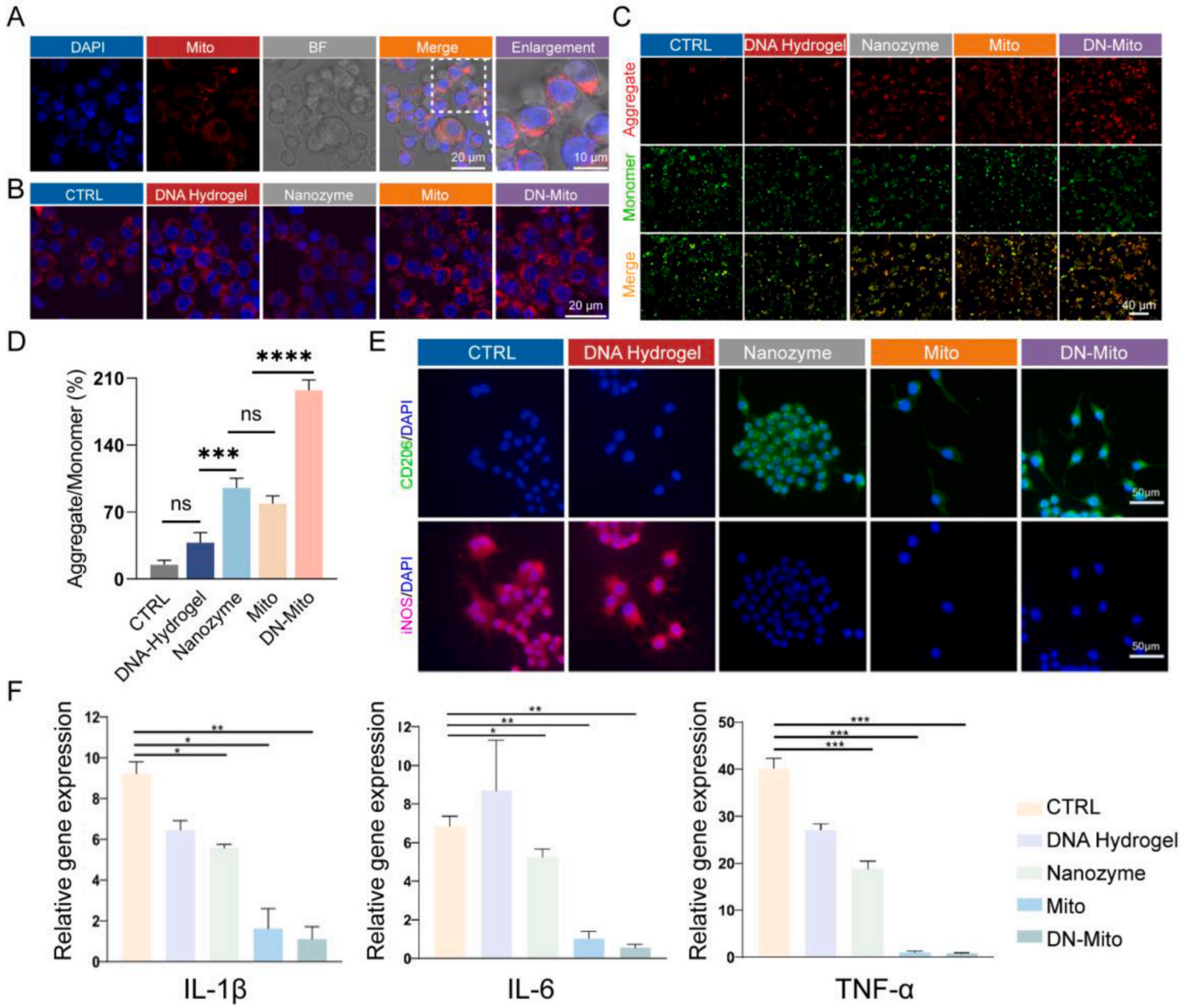

Fig. 4. Mitochondrial Uptake and Immunomodulatory Effects of the Composite Material on Macrophages. (A) Macrophage uptake of mitochondria was assessed by pre-staining the mitochondria with red fluorescence. The images show the internalization of mitochondria by macrophages after treatment, providing a visual representation of the mitochondrial delivery efficiency. (Scale bar: 20 μm). (B) Macrophage mitochondrial fluorescence staining after different treatments, showing the distribution and localization of mitochondria within the cells. (Scale bar: 20 μm). (C) JC-1 assay for assessing mitochondrial membrane potential. LPS-induced mitochondrial damage was induced at a concentration of 100 ng/mL, with the corresponding changes in mitochondrial membrane potential evaluated (Scale bar: 40 μm). (D) Quantification of JC-1 staining results. (E) Immunofluorescence staining of macrophage markers CD206 (M2 macrophage marker) and iNOS (M1 macrophage marker) to assess macrophage polarization. The images highlight the distinct distribution of these markers, indicating the polarization status of macrophages in response to treatments. (Scale bar: 50 μm). (F) qRT-PCR analysis of macrophage inflammatory cytokines IL-1β, IL-6, and TNF-α expression. One-way ANOVA analysis was utilized. *$p < 0.05$, **$p < 0.01$, ***$p < 0.001$ and ****$p < 0.0001$.

exogenous mitochondria in the composite material not only enhanced the anti-inflammatory effects but also presents a promising new material for the treatment of rheumatoid arthritis.

2.3. RNA-seq Verification in Macrophages

Subsequently, we conducted further validation of the experimental findings at the transcriptomic level to substantiate the observed effects. Through transcriptomic analysis, we identified differentially expressed genes between the experimental and control groups. UpSet-R analysis revealed significant changes in gene expression in the Mito group and DN-Mito group (Fig. 5A). These differentially expressed genes provide a foundation for further functional analysis and the exploration of biological mechanisms. The Venn diagram illustrates the relationship between the different treatment groups (Fig. S3A). And 3D PCA (Principal Component Analysis) plot shows the clustering of different treatment groups based on their gene expression profiles (Fig. S3B). The close clustering of the treatment groups, especially in PC1, suggests that there is significant overlap in gene expression, with distinct separation visible for the Mito group and DN-Mito group, reflecting their unique gene expression profile. Therefore, we conducted a more in-depth analysis of the sequencing results for the Mito and DN-Mito groups to further investigate their distinct gene expression patterns.

The enrichment analysis reveals that both Mito and DN-Mito treatments significantly impact immune response regulation and mitochondrial-related processes (Figs. S3C and D). DN-Mito, in

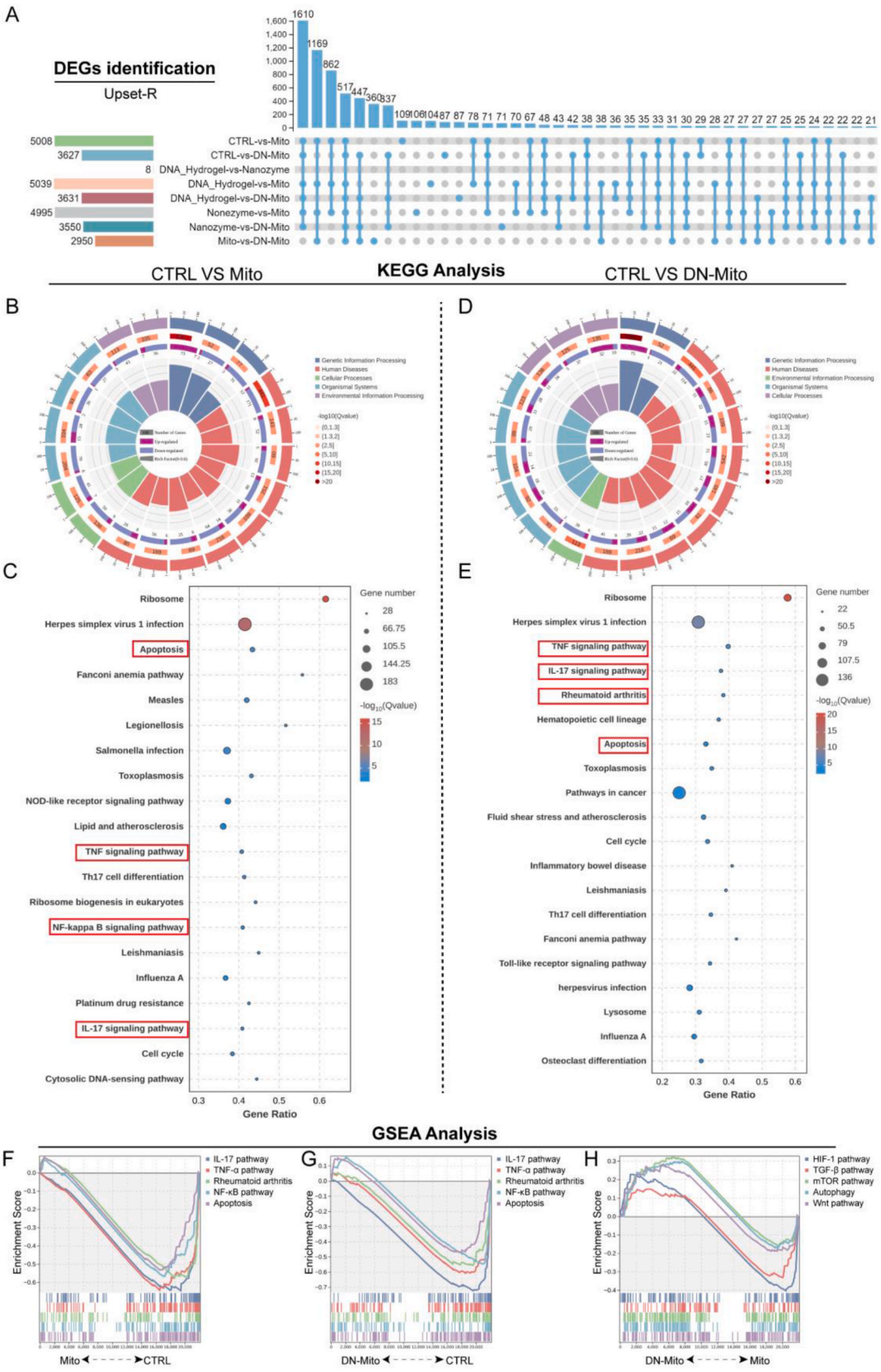

Fig. 5. RNA-seq Verification in Macrophages. (A) DEGs were identified to determine the differential gene sets by all possible combinations of patterns. (B–C) KEGG enrichment circular diagrams showing the top enriched pathways for differentially expressed genes in CTRL vs Mito and CTRL vs DN-Mito groups. (D–E) KEGG significance bubble plots showing the differentially enriched pathways in the CTRL vs Mito and CTRL vs DN-Mito groups. (F–H) KEGG GSEA analysis was performed for all genes across the CTRL vs Mito, CTRL vs DN-Mito, and Mito vs DN-Mito comparison groups.

particular, shows a stronger influence on mitochondrial apoptosis and membrane potential, indicating its potential role in modulating immune and mitochondrial dynamics. KEGG pathway analysis results comparing the control group (CTRL) with the Mito group (Fig. 5B and C) and the DN-Mito group (Fig. 5D and E). Each enrichment circular plot illustrates the top 20 differentially expressed genes involved in various biological pathways. Additionally, we further visualized and compared the specific pathways using enrichment bubble plots to provide a more detailed representation of the differential pathways. Through comparative analysis, it was found that significant alterations occurred in the apoptosis, TNF, IL-17, and NF-κB signaling pathways following Mito and DN-Mito treatment. These pathways are closely associated with inflammation and tissue repair in RA. Notably, a significant change in the rheumatoid arthritis signaling pathway was also observed in the DN-Mito group. Finally, we conducted a detailed GSEA analysis of these key pathways. The results showed that, compared to the CTRL group, gene expression levels in the apoptosis, TNF, IL-17, NF-κB, and rheumatoid arthritis signaling pathways were lower in both the Mito and DN-Mito groups, indicating suppression of these pathways (Fig. 5F and G). Additionally, when comparing the Mito group to the DN-Mito group, we observed enrichment of the HIF-1 and TGF-β signaling pathways in the Mito group, while the mTOR, Autophagy, and Wnt signaling pathways

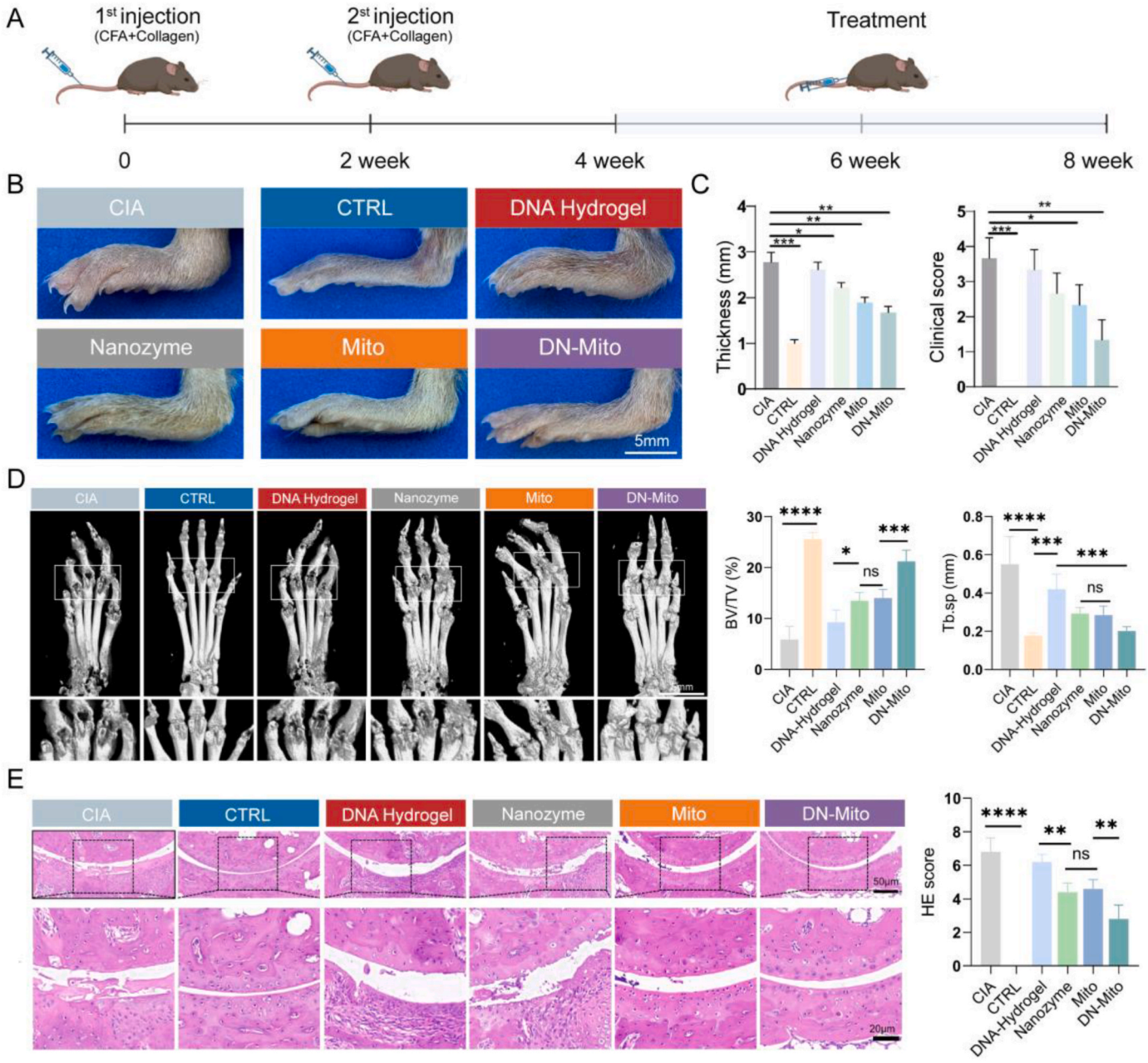

Fig. 6. Therapeutic Efficacy of Composite Material in RA Mouse Model. (A) Schematic diagram of RA model establishment and experimental timeline. (B) Representative images of mouse paws after different in vivo treatments, showing the clinical manifestation of inflammation and edema in the paws of CIA mice. (Scale bar: 5 mm). (C) Measurement of paw thickness and clinical scores for mice in different treatment groups. Paw thickness was quantified to assess the degree of edema, while clinical scores were assigned based on the severity of inflammation and joint damage. (D) Representative micro-CT images of the hind paw in the CIA mouse model, showing bone structure and joint integrity after different treatments, along with quantitative analysis of BV/TV and Tb.sp. (E) Hematoxylin-eosin staining of the ankle joints from mice, along with quantitative analysis to assess joint integrity (Scale bar: 50 μm). n = 5; One-way ANOVA analysis was utilized. *p < 0.05, **p < 0.01, ***p < 0.001 and ****p < 0.0001.

were enriched in the DN-Mito group. This suggests that DN-Mito may offer enhanced therapeutic potential for RA treatment (Fig. 5H).

Taken together, these findings underscore the complementary effects of mitochondrial transfer and nanozyme therapy in modulating key molecular pathways associated with RA. By simultaneously targeting oxidative stress, immune regulation, and mitochondrial dysfunction, this approach holds promise as an effective strategy for comprehensive RA treatment, with the potential for enhanced clinical outcomes. Future studies will be crucial to further validate these molecular targets and explore their impact on long-term disease progression and functional recovery in RA patients.

2.4. *In vivo* therapeutic effects of DN-Mito in collagen-induced arthritis mice

In vivo, we first established a RA mouse model using DBA/1 mice, as depicted in Fig. 6A. This model was successfully validated, and the HE staining of various organs confirmed the good in vivo biocompatibility of the materials across different groups (Fig. S4 A). Over the subsequent month, we conducted therapeutic studies on these RA model mice using different materials. The experimental results demonstrated that mice in the model control group exhibited significant paw swelling. Treatment with nanozymes resulted in a partial reduction in paw swelling, indicating a moderate level of improvement. When exogenous mitochondria were used alone for treatment, there was a further reduction in the severity of paw swelling. Finally, the RA mice treated with the composite material containing mitochondria, DNA hydrogel, and nanozymes showed the most significant reduction in paw swelling. Additionally, the clinical scoring of RA in the mice corresponded with these findings, with the composite material treatment group displaying the lowest clinical scores (Fig. 6B and C).

Next, we utilized micro-computed tomography (micro-CT) to conduct a comprehensive evaluation of bone degradation in the RA model mice. The micro-CT results (Fig. 6D) revealed extensive bone erosion across multiple joints within the feet of the RA model mice. In the group treated with nanozymes, preliminary signs of bone regeneration were observed. This regenerative effect was further enhanced when exogenous mitochondria were administered. Remarkably, the group treated with the composite material, comprising DNA hydrogel, nanozymes, and exogenous mitochondria, exhibited the most pronounced bone restoration. Hematoxylin and eosin (HE) staining (Fig. 6E) confirmed the better bone repair achieved with the composite material treatment, highlighting its potential efficacy in reversing bone damage induced by RA.

To address the excessive secretion of pro-inflammatory cytokines (IL-1β, IL-6, TNF-α) by macrophages, which is a key contributor to the damage of bone, cartilage, and synovial structures in RA, we conducted comprehensive immunohistochemistry (IHC) and immunofluorescence analyses. These analyses aimed to evaluate the effectiveness of different treatment materials in modulating the expression of these inflammatory cytokines. The results of IHC (Fig. 7A and C) demonstrated that treatment with nanozymes significantly reduced the expression levels of IL-6 and TNF-α in inflamed RA tissues. The introduction of exogenous mitochondria further suppressed the expression of these cytokines. Most notably, the combination therapy using a composite material consisting of DNA hydrogel, exogenous mitochondria, and nanozymes led to the most pronounced reduction in IL-6 and TNF-α levels. The findings from immunofluorescence analysis (Fig. 7B and D) were consistent with the IHC results, providing additional confirmation that the composite material incorporating DNA hydrogel, exogenous mitochondria, and nanozymes significantly inhibited the expression of IL-1β and TNF-α. These results underscore the potential of this composite material as an effective therapeutic approach for RA.

3. Discussion

The innovative dual-action strategy combining nanozymes and mitochondrial transfer in a polymer-modified DNA hydrogel platform offers a promising therapeutic approach for RA. This study demonstrates that the co-delivery of Prussian blue nanozymes and mitochondria addresses two key pathological mechanisms of RA, namely chronic inflammation and metabolic dysfunction in immune cells.

The use of DNA hydrogels as a delivery matrix is particularly advantageous due to their excellent biocompatibility, injectability, and ability to encapsulate and release multiple bioactive molecules [16]. Their self-healing properties and shear-thinning behavior make them ideal for minimally invasive joint injection, ensuring optimal delivery to the affected site [17]. Moreover, the capacity of DNA hydrogels to protect encapsulated agents from premature degradation and facilitate sustained release enhances the therapeutic efficacy and reduces the need for frequent administration [18].

Nanozymes, such as Prussian blue, were utilized in this study not only for their well-known ROS scavenging properties but also for their ability to downregulate the expression of key pro-inflammatory cytokines, such as TNF-α and IL-1β [19]. By interfering with the signaling pathways that promote cytokine production, the nanozymes help mitigate the chronic inflammation characteristic of RA, thus protecting joint tissue from further degradation.

A critical aspect of RA pathology involves the metabolic dysfunction of macrophages [20], where impaired mitochondrial function disrupts cellular energy homeostasis and perpetuates inflammatory signaling [21]. In this study, mitochondrial transfer serves as a novel intervention to restore metabolic balance. By delivering purified, healthy mitochondria directly into the joint, this technique aims to replenish the damaged mitochondria within macrophages, thereby enhancing their metabolic flexibility and reducing the production of pro-inflammatory mediators. This restoration of mitochondrial function not only improves the overall metabolic state of the cells but also attenuates the expression of inflammatory cytokines, addressing a root cause of persistent inflammation in RA.

The combined application of nanozymes and mitochondrial transfer was shown to have a synergistic effect, significantly improving therapeutic outcomes compared to either treatment alone. In the collagen-induced arthritis mouse model, the composite hydrogel effectively reduced joint inflammation, cartilage damage, and the expression of pro-inflammatory cytokines, leading to improved overall joint function. This dual-action approach, targeting both inflammation and mitochondrial dysfunction, provides a more comprehensive strategy for managing RA.

Despite these promising results, several challenges remain. Ensuring the long-term stability and integration of transplanted mitochondria, potential immune reactions, and optimizing the dosage and delivery methods for different patient populations require further investigation. The development of live mitochondria-based therapies offers new opportunities, particularly in the context of organoid construction. The ability to incorporate viable mitochondria into 3D organoid models could not only provide insights into mitochondrial function in disease states but also serve as a platform for testing mitochondrial-targeted therapies. However, achieving the efficient incorporation and functional integration of live mitochondria into complex organoid structures presents significant technical hurdles, including the need for precise control over mitochondrial delivery, survival, and activity within the organoid matrix. Future work in this area should focus on optimizing the methods for mitochondrial delivery into organoid systems, ensuring their long-term functionality, and exploring how mitochondrial reprogramming can enhance tissue regeneration.

In conclusion, this study presents a compelling case for the use of a dual-action DNA hydrogel-based therapy in RA treatment. By simultaneously targeting chronic inflammation and metabolic dysfunction in macrophages, this approach offers a novel and effective strategy for

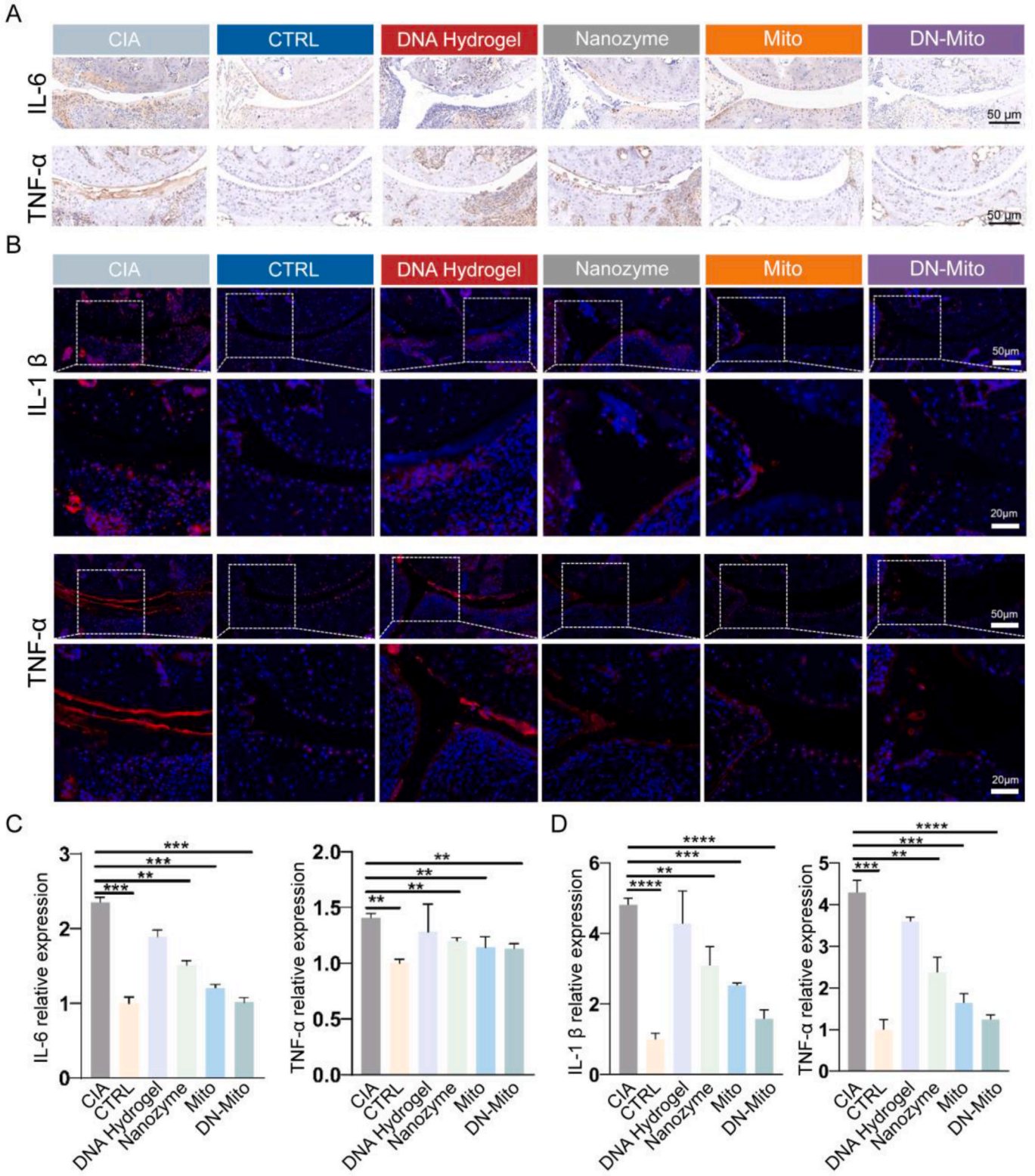

Fig. 7. Histological and Immunofluorescence Staining Showing Therapeutic Effects *In Vivo*. (A) Immunohistochemical staining of IL-6 and TNF-α in different groups after various in vivo treatments, demonstrating the localization and expression levels of these pro-inflammatory cytokines in tissue sections. (Scale bar: 50 μm). (B) Immunofluorescence staining of IL-1β and TNF-α in different groups after various treatments in vivo (Scale bar: 20 μm). (C) Quantitative analysis of immunohistochemistry and immunofluorescence staining in vivo. One-way ANOVA analysis was utilized. *$p < 0.05$, **$p < 0.01$, ***$p < 0.001$ and ****$p < 0.0001$.

managing RA. Based on our preclinical results, particularly the observed ability of the therapy to modulate inflammation and restore mitochondrial function, we believe that this therapy could offer potential therapeutic benefits across various stages of RA, from early to advanced and refractory cases. Further research into mitochondrial therapies, particularly in the context of organoid construction, could complement these strategies, enabling more robust models for disease modeling and therapeutic testing. Future research should focus on refining this technology, exploring its applicability in other inflammatory and degenerative conditions, and ultimately paving the way for clinical translation.

Methods

Cell culture

Bone marrow-derived mesenchymal stem cells (BMSCs) and macrophages (Raw264.7 cell line) were obtained from the Chinese Academy of Sciences Cell Bank. BMSCs were cultured in MEM-alpha medium supplemented with 10 % fetal bovine serum (FBS) and 1 % penicillin-streptomycin to ensure the necessary nutrients and antibiotic protection. The cells were maintained in a humidified incubator at 37 °C with 5 % CO_2. For passaging and seeding, BMSCs were enzymatically dissociated using trypsin and collected via centrifugation. The Raw264.7 was cultured in DMEM supplemented with 10 % FBS. The culture conditions for Raw264.7 cells were similar to those for BMSCs, with the addition of 10 % FBS and 1 % penicillin-streptomycin in the medium to support cell proliferation and prevent bacterial contamination.

Formation of DNA hydrogel

The DNA hydrogel was synthesized through a multi-step process. First, acetylated anchoring DNA was designed and synthesized using solid-phase methods, purified by HPLC, and verified by mass spectrometry. A 40 wt% acrylamide/sodium acrylate mixture was prepared, followed by deoxygenation of reagents. To achieve RGD functionalization, 10 mM of acrylated RGD peptide (sequence: G(acryl-K)GGGRGDSP) was incorporated into the above solution. The reaction system was then set up with acetylated DNA and the acrylamide mixture, initiating polymerization with tetramethylethylenediamine and ammonium persulfate under nitrogen. The reaction was sealed and incubated anaerobically for 12 h to form the DNA-conjugated acrylamide polymer. The polymer was purified by methanol precipitation to remove unreacted monomers. Crosslinking and heat-activated blocking DNA libraries were designed to control DNA interactions, enabling the formation of a stable gel network. Finally, DNA self-assembly gel formation was induced by mixing the libraries and heating to 37 °C, completing the DNA hydrogel synthesis for subsequent applications.

Anchoring DNA strand sequence:/5Acryd/GACGGCTCATAAGGCTC TAATC.

64-splint library: F:TTAGT**N**A**N**T**N**TCCCGATTAGAGCCTTATGAGC CGTC.

R:GGGA**N**A**N**T**N**ACTAAGATTAGAGCCTTATGAGCCGTC

64-heat-activated crosslinkers: F:AAGA**N**A**N**T**N**ACTGT.

R:ACAGT**N**A**N**T**N**TCTT

Mitochondria extraction

BMSCs were used for mitochondrial extraction, with cells expanded beforehand. After gently resuspending the cell pellet in pre-chilled PBS on ice, a small portion was set aside for counting. The remaining cells were centrifuged at 600 g for 5 min at 4 °C, and the supernatant was discarded. Mitochondrial isolation reagent (1–2.5 ml) was added to 20–50 million cells, followed by gentle resuspension and incubation on ice for 10–15 min. The cell suspension was then homogenized using approximately 15 strokes. The efficiency of homogenization was checked by mixing 2 μL of the homogenate with trypan blue and observing the proportion of stained cells under a microscope. If less than 50 % of cells were stained, additional homogenization was performed until the desired level was reached. Once over 50 % of cells were stained, homogenization was stopped to avoid mitochondrial damage. The homogenate was centrifuged at 600 g for 10 min at 4 °C to remove debris, followed by a second centrifugation at 11,000 g for 10 min. The resulting pellet contained the isolated mitochondria.

Synthesis of prussian blue nanozymes

In this study, Prussian blue nanozymes were synthesized using a classic chemical precipitation method. Initially, 8 g of polyvinylpyrrolidone (PVP) was used as a stabilizer and mixed with 696 mg of potassium ferricyanide ($K_3[Fe(CN)_6]$) to form the initial reaction mixture. This mixture was then combined with 50 mL of 1 M hydrochloric acid (HCl) solution to initiate the formation of Prussian blue. The mixture was stirred at room temperature for 1 h to ensure complete reaction, followed by heating at 80 °C for 24 h to facilitate the formation of the nanozymes.

After the synthesis, the product was washed five times with deionized water to remove unreacted starting materials and by-products. Each washing step was followed by high-speed centrifugation at 30,000 rpm for 10 min to collect the nanoparticles. This method resulted in Prussian blue nanozymes with good dispersion and stability.

Mitochondrial membrane potential assay

For each well in a 6-well plate, first remove the culture medium. Wash the cells once with PBS solution, then add 1 ml of fresh cell culture medium to each well. Subsequently, add 1 ml of JC-1 staining solution to each well, ensuring thorough mixing. Place the 6-well plate in a cell incubator and incubate at 37 °C for 20 min to allow the JC-1 dye to interact with the cells. After incubation, gently aspirate the supernatant and wash the cells twice with JC-1 specific buffer to remove any unbound dye. Next, add 2 ml of cell culture medium to each well. Finally, observe and record the JC-1 staining results using a laser confocal microscope. High mitochondrial membrane potential is indicated by red fluorescence, whereas low membrane potential is indicated by green fluorescence.

CCK-8 proliferation assay

The experiment was divided into five groups: control, DNA hydrogel, nanozyme, mitochondria, and composite material (DNA hydrogel + nanozyme + mitochondria). To prepare the extracts, the DNA hydrogel and composite material groups were mixed with serum-free culture medium and incubated at 37 °C in a 5 % CO_2 incubator for 48 h. Macrophages were then seeded into a 96-well plate, ensuring consistent cell numbers across three replicates for each group to maintain experimental accuracy and reproducibility. Each group was cultured under its respective conditions for 48 h, followed by the addition of 10 μl of CCK-8 reagent to each well containing 100 μl of culture medium. After a 2-h incubation, optical density (OD) at 450 nm was measured using a microplate reader, with precautions taken to minimize light exposure and reduce potential measurement errors.

Modeling and clinical scoring

To establish a collagen-induced RA mouse model, 6-week-old male DBA/1j mice were used. An initial emulsion was prepared by mixing type II collagen (2 mg/mL) with complete Freund's adjuvant (CFA, 1 mg/mL) in a 1:1 ratio, and 100 μL of this emulsion was subcutaneously injected to induce the primary immune response. Two weeks later, a

booster emulsion was prepared by mixing type II collagen (2 mg/mL) with incomplete Freund's adjuvant (IFA, 1 mg/mL) in the same ratio, and 100 μL was injected subcutaneously into the tail. The collagen-induced arthritis (CIA) model was successfully established four weeks after the initial immunization. Joint destruction and mobility were assessed using a clinical scoring system: 0 points indicated no joint destruction and normal mobility; 1 point indicated minimal, localized bone erosion; 2 points indicated mild to moderate erosion in a confined area; 3 points indicated significant, widespread erosion; and 4 points indicated extensive destruction affecting the overall joint structure.

Micro-CT analysis

Joint samples were gently rinsed with deionized water to remove any residual fixative. The samples were then placed securely on the sample holder of the Micro-CT scanner, ensuring stable and proper positioning. After scanning, the raw data were reconstructed using NRecon software to generate images, followed by 3D reconstruction using CTVol software to produce three-dimensional visualizations.

Statistical analysis

Data are presented as the mean ± standard deviation (SD). Statistical analysis was performed using one-way analysis of variance (ANOVA), followed by post hoc tests for multiple comparisons to identify differences between groups. A P-value of less than 0.05 was considered statistically significant. Specific significance levels were denoted as follows: * for $P < 0.05$, ** for $P < 0.01$, and *** for $P < 0.001$.

CRediT authorship contribution statement

Fuxiao Wang: Writing – original draft, Methodology, Investigation, Formal analysis, Data curation, Conceptualization. **Yafei Han:** Resources, Methodology, Data curation. **Qirong Zhou:** Methodology, Formal analysis, Data curation. **Shihao Sheng:** Methodology, Data curation. **Yan Hu:** Supervision, Software. **Hao Zhang:** Visualization, Validation. **Xiao Chen:** Software. **Chongru He:** Writing – review & editing, Resources, Conceptualization. **Hongbo Tan:** Supervision, Formal analysis. **Long Bai:** Writing – review & editing, Resources, Conceptualization. **Jiacan Su:** Writing – review & editing, Supervision, Funding acquisition, Conceptualization.

Ethics approval and consent to participate

The Ethics of this experiment was approved by the Ethics Review Committee of Shanghai University (YS 2024-165).

Declaration of Competing Interests

The authors declare that there are no financial conflicts of interest or personal relationships that could have influenced the outcomes of this study.

Acknowledgments

This work was financially supported by National Natural Science Foundation of China (32471396, 82230071, 82172098), Shanghai Committee of Science and Technology (23141900600, Laboratory Animal Research Project), Shanghai Clinical Research Plan of SHDC2023CRT01, Shanghai Municipal Demonstration Project for Innovative Medical Device Applications (23SHS05700), Young Elite Scientist Sponsorship Program by China Association for Science and Technology (YESS20230049), Key Project of the Seed Program for Medical New Technology Research and Translation of the Shanghai Municipal Health Commission (2024ZZ1001).

Appendix A. Supplementary data

Supplementary data to this article can be found online at https://doi.org/10.1016/j.bioactmat.2024.12.027.

References

[1] W.P. Arend, G.S. Firestein, Pre-rheumatoid arthritis: predisposition and transition to clinical synovitis, Nat. Rev. Rheumatol. 8 (2012) 573–586.
[2] S. Alivernini, G.S. Firestein, I.B. McInnes, The pathogenesis of rheumatoid arthritis, Immunity 55 (2022) 2255–2270.
[3] A. Finckh, et al., Treatment of very early rheumatoid arthritis with symptomatic therapy, disease-modifying antirheumatic drugs, or biologic agents: a cost-effectiveness analysis, Ann. Intern. Med. 151 (2009) 612–621.
[4] Y. Zhao, et al., Supramolecular adhesive hydrogels for tissue engineering applications, Chem. Rev. 122 (2022) 5604–5640.
[5] R. Dimatteo, N.J. Darling, T. Segura, In situ forming injectable hydrogels for drug delivery and wound repair, Adv. Drug Deliv. Rev. 127 (2018) 167–184.
[6] S. Ren, et al., Nanotechnology-empowered combination therapy for rheumatoid arthritis: principles, strategies, and challenges, J. Nanobiotechnol. 22 (2024) 431.
[7] D. Jiang, et al., Nanozyme: new horizons for responsive biomedical applications, Chem. Soc. Rev. 48 (2019) 3683–3704.
[8] X. Ye, et al., Reactive oxygen/nitrogen species scavenging multi-enzyme mimetic ultrasmall calcium hexacyanoferrate (III) nanozyme for hypertension remedy, Mater. Today 68 (2023) 148–163.
[9] L. Zhang, H. Wang, X. Qu, Biosystem-inspired engineering of nanozymes for biomedical applications, Adv. Mater. 36 (2024) 2211147.
[10] L. Zhang, et al., Nanoenzyme engineered neutrophil-derived exosomes attenuate joint injury in advanced rheumatoid arthritis via regulating inflammatory environment, Bioact. Mater. 18 (2022) 1–14.
[11] C.M. Weyand, J.J. Goronzy, The immunology of rheumatoid arthritis, Nat. Immunol. 22 (2021) 10–18.
[12] J. Falconer, et al., Synovial cell metabolism and chronic inflammation in rheumatoid arthritis, Arthritis Rheumatol. 70 (2018) 984–999.
[13] R. Giwa, J.R. Brestoff, Mitochondria transfer to CD4+ T cells may alleviate rheumatoid arthritis by suppressing pro-inflammatory cytokine production, Immunometabolism 4 (2022) e220009.
[14] T. Huang, T. Zhang, J. Gao, Targeted mitochondrial delivery: a therapeutic new era for disease treatment, J. Contr. Release 343 (2022) 89–106.
[15] R.-Z. Lin, et al., Mitochondrial transfer mediates endothelial cell engraftment through mitophagy, Nature 629 (2024) 660–668, https://doi.org/10.1038/s41586-024-07340-0.
[16] Y. Han, et al., Heterogeneous DNA hydrogel loaded with Apt02 modified tetrahedral framework nucleic acid accelerated critical-size bone defect repair, Bioact. Mater. 35 (2024) 1–16.
[17] S. Correa, et al., Translational applications of hydrogels, Chemical reviews 121 (2021) 11385–11457.
[18] J. Gačanin, C.V. Synatschke, T. Weil, Biomedical applications of DNA-based hydrogels, Adv. Funct. Mater. 30 (2020) 1906253.
[19] X. Bao, J. Zhao, J. Sun, M. Hu, X. Yang, Polydopamine nanoparticles as efficient scavengers for reactive oxygen species in periodontal disease, ACS Nano 12 (2018) 8882–8892.
[20] U. Fearon, M. Canavan, M. Biniecka, D.J. Veale, Hypoxia, mitochondrial dysfunction and synovial invasiveness in rheumatoid arthritis, Nat. Rev. Rheumatol. 12 (2016) 385–397.
[21] U. Fearon, M.M. Hanlon, A. Floudas, D.J. Veale, Cellular metabolic adaptations in rheumatoid arthritis and their therapeutic implications, Nat. Rev. Rheumatol. 18 (2022) 398–414.